Korean J. Chem. Eng., 39(7), 1968-1974 (2022)
DOI: 10.1007/s11814-021-1007-x

pISSN: 0256-1115
eISSN: 1975-7220

Enhanced electrical conductivity and electromagnetic shielding efficiency of epoxy resin using graphene nanoplatelets

Wei Dong*, Miao Zhao, Fan-Long Jin*,†, and Soo-Jin Park***,†**

*Department of Polymer Materials, Jilin Institute of Chemical Technology, Jilin City 132022, P. R. China
**Jilin Jiuhua Foreign Affairs School, No. 100 Huanxie Road, Chuanying District, Jilin City 132012, P. R. China
***Department of Chemistry, Inha University, Nam-gu, Incheon 22212, Korea
(*Received 26 September 2021 • Revised 3 November 2021 • Accepted 8 November 2021*)

Abstract−Graphene nanoplatelets (GNPs) employed as conductive fillers were added to an epoxy matrix, diglycidylether of bisphenol-A (DGEBA), to enhance the electrical conductivity and electromagnetic shielding efficiency of DGEBA. In addition, we investigated the influence of GNP fraction on the thermal properties, flexural strength, impact strength, electrical conductivity, electromagnetic shielding efficiency, and morphology of DGEBA/GNP nanocomposites. The electrical properties indicated that the electrical conductivity of DGEBA/GNP nanocomposites consisting of higher than 7.5 wt% GNPs was significantly improved compared to that of pristine DGEBA. The electromagnetic shielding efficiency of the nanocomposite showed a maximum value of 3.87 dB at 10 wt% GNPs, which is 287% higher than that of pristine DGEBA. An analysis of the fracture surfaces of the nanocomposites showed a rough morphology with numerous micro-cracks. In addition, the GNPs in the DGEBA matrix were stacked and formed a continuous conductive path at high GNP contents.

Keywords: Epoxy Resin, Graphene Nanoplatelets, Conductive Filler, Electrical Conductivity, Electromagnetic Shielding Efficiency

INTRODUCTION

Electronic information technology has brought convenience to people's lives. Simultaneously, however, electromagnetic interference affects daily life, military activities, and even space exploration [1-4]. Therefore, to protect human health and ensure data security and electromagnetic pulse protection of military equipment, it is necessary to develop electromagnetic shielding materials that can absorb or shield electromagnetic waves to address such adverse effects [5-7].

Electromagnetic shielding materials are mainly divided into three categories: metal and its alloy-based electromagnetic shielding materials [8], foam materials [9], and conductive composite materials [10]. Among them, polymer-based conductive composite materials are lightweight and exhibit good corrosion resistance [11]. Research on electromagnetic shielding composite materials can be divided into surface conductive type and filling type. Metal fusion, surface plating, and conductive coatings are commonly used to prepare surface conductive-type materials [12]. The filling-type electromagnetic shielding composite materials are mainly fabricated by adding conductive and magnetic conductive fillers into polymers [13].

Epoxy resin has a low curing shrinkage rate, high bonding strength, good chemical stability, high mechanical strength, and good electrical insulating performance. Owing to these properties, epoxy resin has wide applications in automobiles, optical machinery, aerospace, aircraft, building materials, paint, adhesives, sports equipment, engineering plastics, composite materials, and electronic materials [14-16]. However, it is difficult for the epoxy resin to meet the electromagnetic shielding requirements as an electrical insulating material. The most common solution is to introduce highly conductive fillers into the epoxy matrix. The conductive fillers used in the epoxy resin-based electromagnetic shielding materials include metal fillers, carbon fillers, and compound fillers [17-21].

Among these fillers, graphene has sp^2 hybridization and a lattice-like monolayer of carbon atoms packed tightly together. It exhibits comprehensive and excellent performance, including excellent chemical stability and good mechanical, electrical, and thermal properties. Moreover, it exhibits excellent charge transfer performance with electron mobility as high as 1.5×10^3 $cm^2/(V\cdot s)$, which is ten-times higher than that of commercial silicon. The thermal conductivity of graphene can reach 5×10^3 $W/(m\cdot K)$, which is three-times higher than that of diamond. Its strength is up to 130 GPa, which is 100 times higher than that of steel. Therefore, graphene is more likely to meet the requirements of being lightweight, thin, strong, and wide compared to traditional absorbing materials. Moreover, it is expected to break through its limitations and become a novel absorbing material [22-24].

In recent years, many researchers have investigated the preparation and characterization of epoxy resins/graphene nanoplatelet (GNP) nanocomposites [25-36]. Table 1 summarizes the effect of GNPs on the electrical conductivity and electromagnetic shielding efficiency of epoxy-based nanocomposites prepared by various processing procedures.

In the present study, diglycidylether of bisphenol-A (DGEBA)/

†To whom correspondence should be addressed.
E-mail: jinfanlong@163.com, sjpark@inha.ac.kr

Table 1. Electrical conductivity and electromagnetic shielding efficiency of epoxy-based nanocomposites with graphene fillers

Graphene characteristics	Graphene amount	Epoxy matrix	Processing method	Electrical conductivity (S/m)	ESE (dB)	Ref.
No data	0.25 wt% (0.25 wt% TiO_2)	Epoxy resin (Cam Coat 2051) cured with HY591	Melt blending	No data	11	[25]
Thickness >5 nm	2.3 vol%	DGEBA cured with Jeffamine 400	Layer-by-layer method	10^{-4}	No data	[26]
Three-dimensional graphene foams	0.39 wt%	DGEBA cured with amine	In-situ chemical polymerization	3.6	No data	[27]
Thickness <4 nm	12 wt%	DGEBA cured with diethyltoluene diamine	Three-roll miller	10^{-5}	No data	[28]
Thickness: 3-4 nm	2 vol%	DGEBA cured with Jeffaimne D 230	Solution blending	10^{-5}	No data	[29]
Thickness: 8 nm	7 wt%	DGEBA cured with dimer acid	Solution blending	10^{-3}	28.3	[30]
Thermally annealed graphene aerogel	1.2 wt%	bisphenol F epoxy resin cured with ethylenediamine	Melt blending	2.35	10	[31]
Three-dimensional graphene aerogels	0.33 wt%	DGEBA cured with methyl hexahydrophthalic anhydride	Vacuum-assisted impregnation process	73	35	[32]
Thickness: 4-20 nm	0.3 wt%	DGEBA cured with polyetheramine D-230	Melt blending	8×10^{-5}	No data	[33]
No data	7 vol%	DGEBA cured with Jeffamine D-2000	Solution blending	10^{-2}	No data	[34]
Thickness <3 nm	2 vol%	DGEBA cured with Jeffamine 230	Melt blending	10^{-3}	No data	[35]
Thickness: 3 nm	2 vol%	DGEBA cured with Jeffamine 400	Solution blending	10^{-3}	No data	[36]

Note: ESE, electromagnetic shielding efficiency.

GNP nanocomposites were prepared via solution blending using DGEBA as a polymer matrix and GNPs as a conductive filler. The influence of the GNP fraction on the thermal properties, flexural strength, impact strength, electrical conductivity, electromagnetic shielding efficiency, and morphology of the nanocomposites was investigated.

EXPERIMENTAL

1. Materials

The polymer matrix DGEBA (epoxy equivalent weight of 184-195 g/mol) was supplied by Nantong Xingchen Synthetic Material Co., Ltd. The curing agent methyl hexahydrophthalic anhydride (MHHPA) was purchased from Guangzhou Qihua Chemical Co., Ltd. The tris(dimethylaminomethyl)phenol (DMP-30) as a curing accelerator was supplied by Changzhou Runxiang Chemical Co., Ltd. The GNPs with a carbon content of 97.1 wt% were obtained from Yantai Sinagraphene Co., Ltd. Fig. 1 shows the surface morphology of the GNPs.

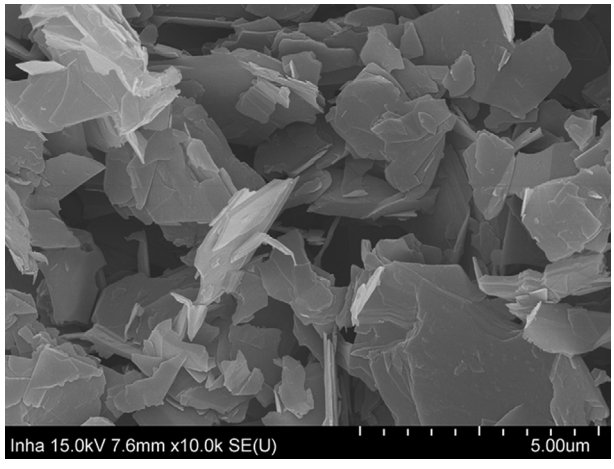

Fig. 1. SEM micrograph of GNPs (magnification of 10000, scale bar of 5 mm).

2. Sample Preparation

The preparation procedure of the DGEBA/GNP nanocomposites is shown in Fig. 2. The GNP content was varied from 0 to 10 wt%. Thereafter, 30 g of DGEBA was heated to 60 °C, and a designed amount of GNPs was added to DGEBA. The mixture was

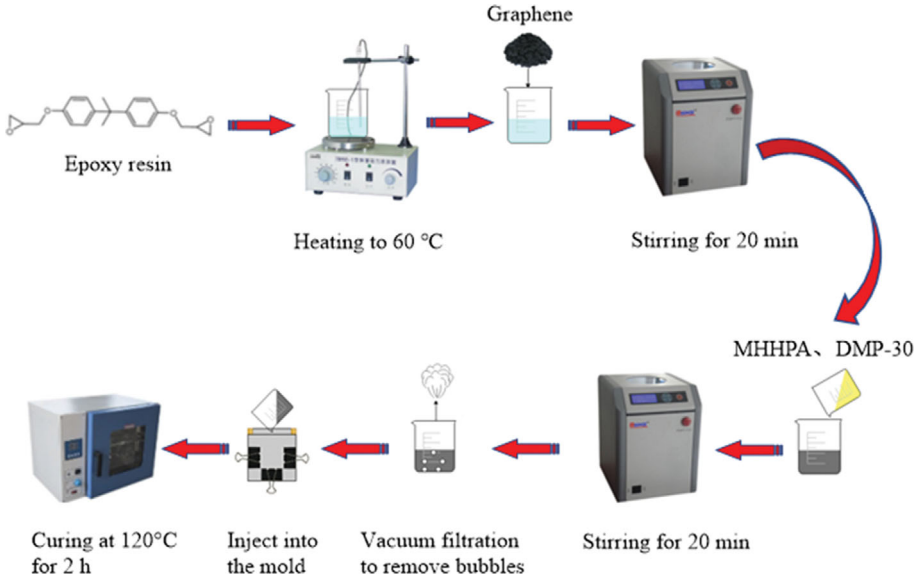

Fig. 2. Schematic illustration of preparation of the DGEBA/GNP nanocomposites.

mixed at 25 °C for 20 min using a planetary mixer, and then an equivalent ratio of MHHPA and DMP-30 was added to the mixture. The mixture was stirred at 25 °C for 20 min using a planetary mixer and then was evacuated at 80 °C for 30 min under reduced pressure. The mixture was injected into a mold sprayed with a mold-release agent and cured at 120 °C for 2 h.

3. Thermogravimetric Analysis

The thermal stability of the DGEBA/GNP nanocomposites was investigated using a TGA instrument (TA Instruments, Q50) from 30 °C to 800 °C at a heating rate of 10 °C/min under a N_2 flow of 30 mL/min.

4. Flexural Strength Tests

The flexural strength of the nanocomposites was measured using a mechanical testing apparatus (WDW 3010) according to the method specified in the standard GB/T 9341-2008. The sample size was 5×10×100 mm^3 and the cross-head speed was 2 mm/min. The flexural strength (σ_f) was calculated using the following equation:

$$\sigma_f = \frac{3PL}{2bd^2} \quad (1)$$

where P is the applied load (in N), L is the span length (in mm), b is the width of the specimen (in mm), and d is the thickness of the specimen (in mm). All the mechanical property values were obtained by averaging five experimental values.

5. Impact Strength Tests

The impact strength of the nanocomposites was measured using an Izod Impact tester (TP04G-S1) in accordance with the method specified in the standard GB/T 1843-2008. The sample size was 5×10×50 mm^3, and the pendulum energy was 5.5 J. The impact strength values were obtained by averaging five experimental values.

6. Electrical Conductivity Tests

The electrical conductivity of the nanocomposites was investigated using a resistivity tester (AT518) in accordance with the method specified in the standard GB/T 1410-2006. The sample size was 5×20×30 mm^3. The electrical conductivity (σ) was calculated using the following equation:

$$\sigma = \frac{L}{RS} \quad (2)$$

where L is the sample thickness, R is the measured resistivity, and S is the cross-sectional area of the sample. The electrical conductivity values were obtained by averaging five experimental values.

7. Electromagnetic Shielding Efficiency Tests

The electromagnetic shielding efficiency of the nanocomposites was measured by a Vector network analyzer (E5071C) according to the method specified in the standard GB/T 32596-2016 [37,38]. The ratio of the nanocomposites to paraffin and the frequency are 1 : 3 and 2-18 GHz, respectively. The electromagnetic shielding efficiency values were obtained by averaging the three experimental values.

8. Microscopic Morphology Analysis

The fracture surfaces of the nanocomposites after the impact strength tests were investigated using thermal field-emission scanning electron microscopy (TFE-SEM, JSM-7610FPlus, JEOL Ltd.).

RESULTS AND DISCUSSION

1. Thermal Stability

The thermal stability of the DGEBA/GNP nanocomposites was investigated through TGA, and the TGA thermograms are shown in Fig. 3. Thermal stability factors, such as the decomposition temperature for 10% weight loss ($T_{10\%}$), decomposition temperature for 50% weight loss ($T_{50\%}$), and char yield at 800 °C were determined from the TGA thermograms [39,40], and the corresponding characteristic data are listed in Table 2.

The $T_{10\%}$ value of the DGEBA/GNP nanocomposites increased with the addition of the GNPs. The $T_{50\%}$ value of the nanocomposites was similar to that of pristine DGEBA. In addition, the char yield at 800 °C of the nanocomposites increased from 3.2 to 15.4% with the increasing GNP content from 0 to 10 wt%. These results

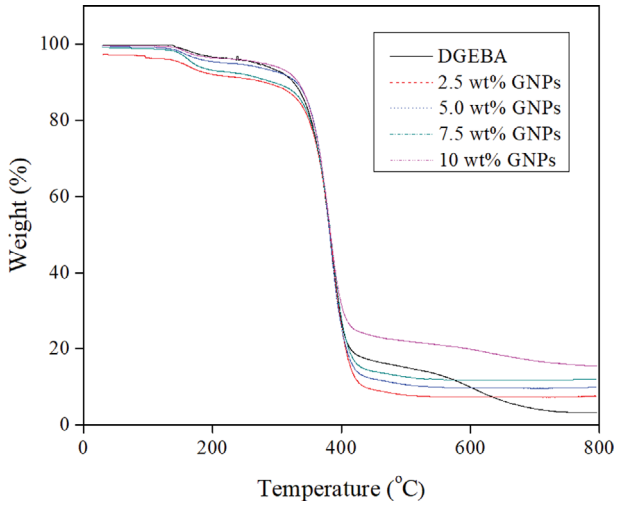

Fig. 3. TGA thermograms of DGEBA/GNP nanocomposites as a function of GNP content.

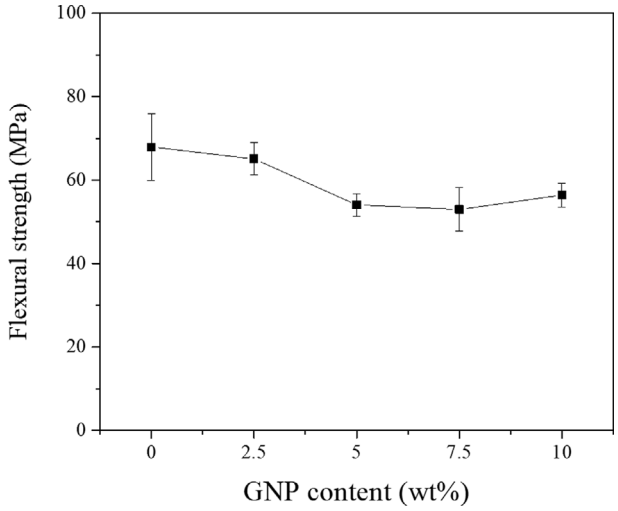

Fig. 4. Flexural strength of DGEBA/GNP nanocomposites as a function of GNP content.

indicate that the addition of the GNPs slightly increased the thermal stability of the nanocomposites. These results can be attributed to better heat capacity and thermal resistance of the GNPs compared to pristine epoxy resin [41,42].

2. Flexural Property

The flexural property of the DGEBA/GNP nanocomposites was studied via flexural strength measurement. Fig. 4 shows the flexural strength of the nanocomposites as a function of the GNP fraction. The flexural strength of DGEBA decreased gradually with the addition of the GNPs. This result can be attributed to the dispersion of graphene in the epoxy matrix that begins to deteriorate, and the graphene in the epoxy matrix forms aggregates at high GNP contents [43]. Therefore, the flexural strength of the DGEBA/GNP composites decreased with the addition of the GNPs.

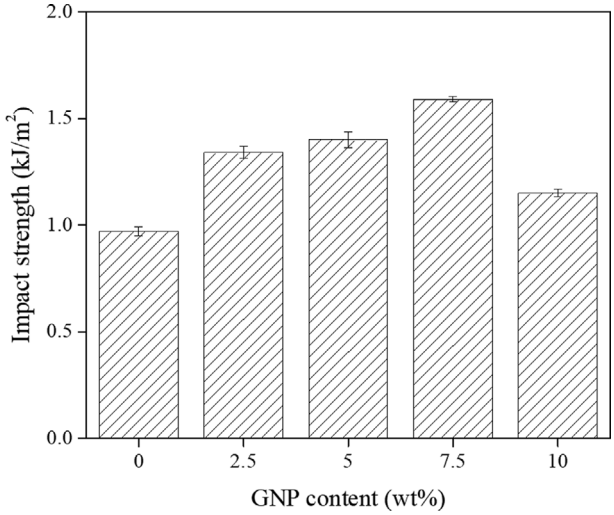

Fig. 5. Impact strength of DGEBA/GNP nanocomposites as a function of GNP content.

3. Impact Strength

Fig. 5 shows the impact strength of the DGEBA/GNP nanocomposites as a function of the GNP content. The pristine DGEBA, which is classified as a brittle material, shows a low impact strength value of 0.97 kJ/m^2 at room temperature [44]. While the impact strength of the nanocomposites increased with the addition of the GNPs, when the GNP content was 7.5 wt%, the impact strength of the nanocomposite was 1.59 kJ/m^2, which is 63% higher than that of pristine DGEBA. This result can be attributed to the absorption of external energy by the micro-cracks generated by the GNP dispersed in the DGEBA matrix [45]. However, the impact strength of the nanocomposites decreased above 7.5 wt% of the GNPs due to the agglomeration of the GNPs and stress concentration induced by stacked GNPs in the epoxy matrix at high GNP content.

4. Electrical Property

Fig. 6 shows the electrical conductivity of the DGEBA/GNP nanocomposites as a function of GNP content. The electrical conductivity

Table 2. Thermal stability factors of DGEBA/GNP nanocomposites obtained from TGA thermograms

GNP content (wt%)	$T_{10\%}$ (°C)[a]	$T_{50\%}$ (°C)[a]	Char yield at 800 °C (%)[b]
0	325.8	382.3	3.2
2.5	326.2	382.8	7.1
5	330.1	382.1	10.0
7.5	331.1	383.4	12.9
10	333.2	383.5	15.4

Note: (a) $T_{10\%}$, $T_{50\%}$, and char yield at 800 °C determined from TGA thermograms; (b) T_g determined from the TMA curves.

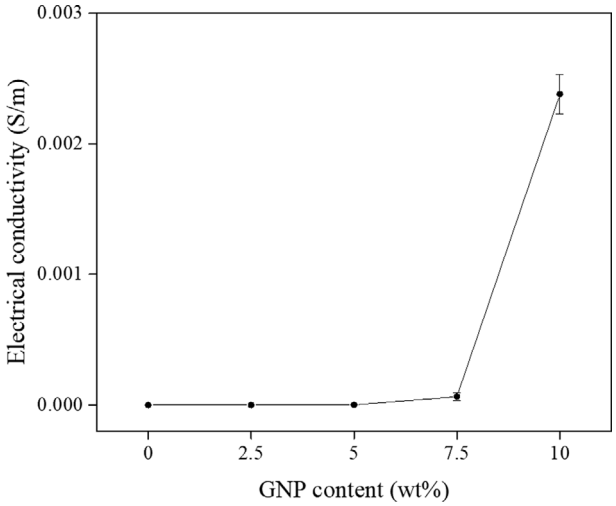

Fig. 6. Electrical conductivity of DGEBA/GNP nanocomposites as a function of GNP content.

of pristine DGEBA was approximately 0, indicating that DGEBA is an insulating material. The electrical conductivity of the nanocomposites was enhanced with the addition of the GNPs. When the GNP content was below 5 wt%, the electrical conductivity of the nanocomposites was slightly higher than that of pristine DGEBA, because the GNPs dispersed in the epoxy matrix did not form a conductive network. When the GNP content was above 7.5 wt%, the electrical conductivity of the nanocomposites improved significantly compared to that of pristine DGEBA, which was due to the formation of a local conductive network by a small number of GNP links. When the GNP content was 10 wt%, the electrical conductivity of the nanocomposites reached a maximum value of 2.38×10^{-3} S/m. This result can be attributed to the formation of an electrically conductive network by the GNPs in the epoxy matrix, leading to a significant increase in the electrical conductivity of the DGEBA/GNP nanocomposites [46-48].

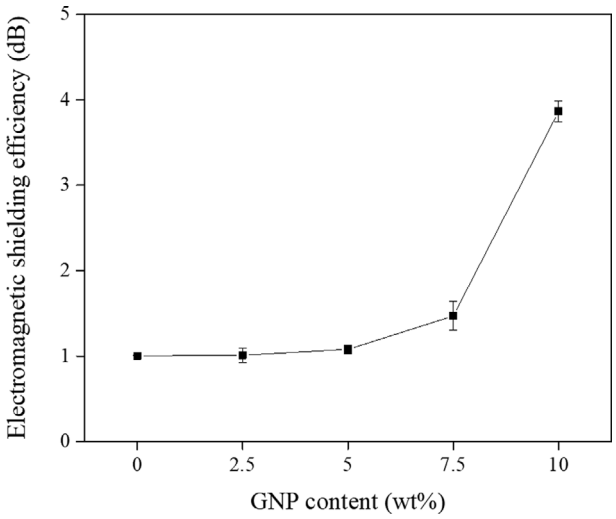

Fig. 7. Electromagnetic shielding efficiency of DGEBA/GNP nanocomposites as a function of GNP content.

5. Electromagnetic Shielding Efficiency

Fig. 7 shows the electromagnetic shielding efficiency of the DGEBA/GNP nanocomposites as a function of the GNP content. The electromagnetic shielding efficiency of pristine DGEBA was 1.0 dB, which indicates that pristine DGEBA almost does not absorb electromagnetic waves. The electromagnetic shielding efficiency of the nanocomposites increased slightly with the increasing GNP content up to 5 wt%. When the GNP content was higher than 5 wt%, the electromagnetic shielding efficiency of the nanocomposites increased significantly and showed a maximum value of 3.87 dB at 10 wt% GNPs, which is 287% higher than that of pristine DGEBA. This result can be attributed to the formation of an electrically conductive network by the GNPs in the epoxy matrix; thus, the electromagnetic waves were reflected and absorbed repeatedly while transferring the GNPs in the electrically conductive network [49,50].

6. Morphological Analysis

The morphology of the DGEBA/GNP nanocomposites was investigated using SEM. Fig. 8 shows the SEM images of the fracture surfaces of the nanocomposites after the impact strength tests. As shown in Fig. 8(a), pristine DGEBA exhibited a mirror-like morphology with ordered cracking behavior due to its poor resistance against crack initiation and propagation, indicating that DGEBA is a brittle material with low impact strength [51].

In contrast, the SEM image of the DGEBA/GNP nanocomposites shows a rough morphology with numerous micro-cracks, indicating plastic deformation prior to the fracture. For a GNP content of 2.5 wt%, 5 wt%, and 7.5 wt%, the nanocomposite exhibited a rough and disordered fracture surface with numerous micro-cracks, as shown in the cross-section SEM micrograph (Fig. 8(b)-(d)). The GNPs embedded in the DGEBA matrix forced the propagating cracks to be disorderly disseminated, generating many new surfaces and increasing the required strain energy [52]. At this point, the GNPs in the DGEBA matrix could not form a continuous conductive path due to the low amount of GNPs.

When the GNP content was further increased to 10 wt%, the GNPs in the DGEBA matrix were stacked and became the point of stress concentration. Thus, the fracture surfaces of the nanocomposites showed numerous layer breakages and micro-cracks during the fracture process, as shown in Fig. 8(e)-(f). At this point, the stacked platelets formed particles and induced more interlayer channels, forming a continuous conductive path in a local. As a result, the electrical conductivity and electromagnetic shielding efficiency of the nanocomposites were enhanced [50,53].

CONCLUSIONS

DGEBA/GNP nanocomposites were prepared via solution blending, and their thermal properties, flexural strength, impact strength, electrical conductivity, electromagnetic shielding efficiency, and morphology were investigated. The thermal stability of the nanocomposites was slightly higher than that of pristine DGEBA. The flexural strength of the nanocomposites decreased gradually with the addition of the GNPs. The impact strength of the nanocomposites at 7.5 wt% was 1.59 kJ/m^2, which is 63% higher than that of pristine DGEBA. The electrical conductivity of the DGEBA/GNP nanocomposites above 7.5 wt% of the GNPs was significantly improved

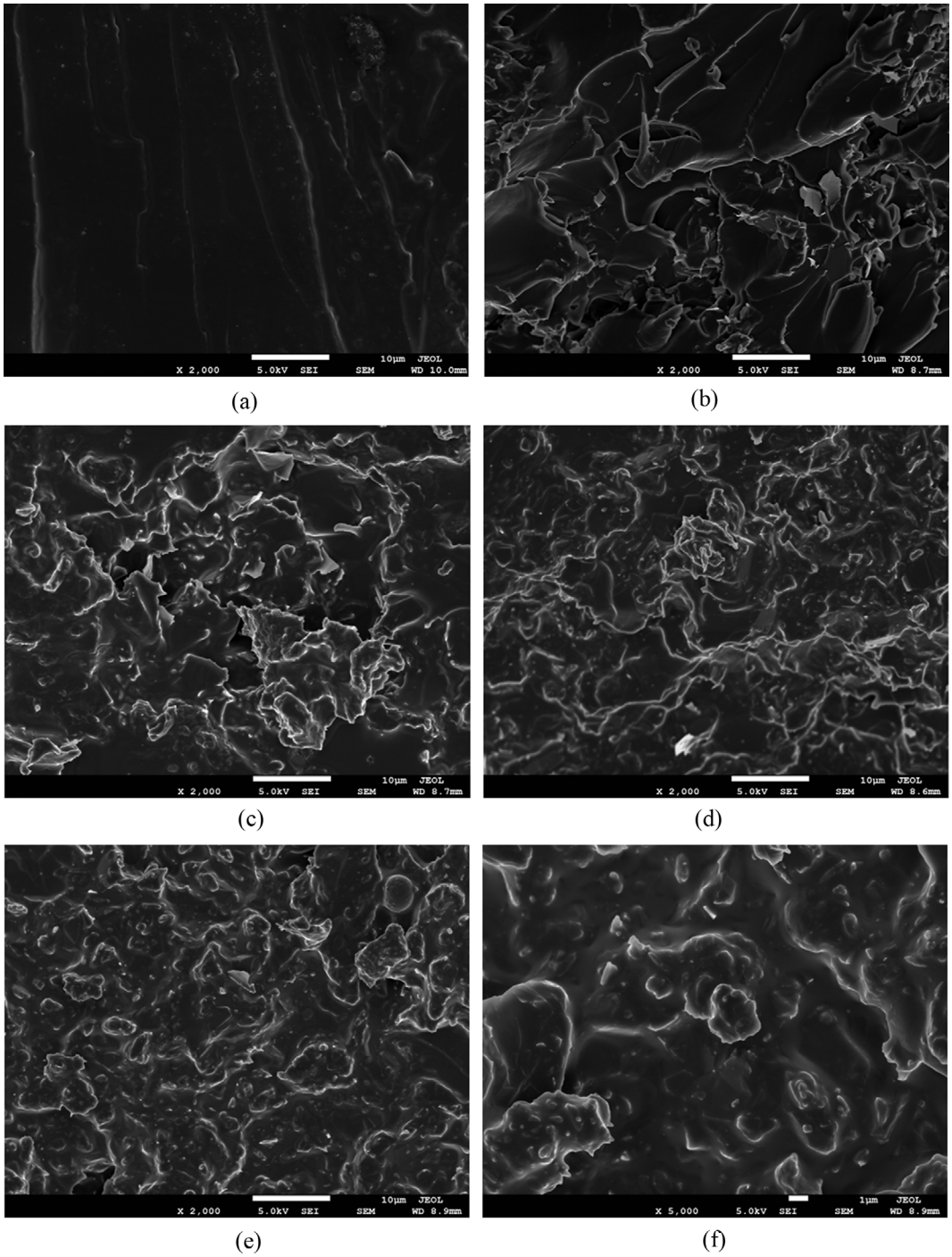

Fig. 8. SEM micrographs of DGEBA/GNP nanocomposites after the impact strength tests: (a) pristine DGEBA (magnification of 2000, scale bar of 10 μm); (b) 2.5 wt% GNPs (magnification of 2000, scale bar of 10 μm); (c) 5.0 wt% GNPs (magnification of 2000, scale bar of 10 μm); (d) 7.5 wt% GNPs (magnification of 2000, scale bar of 10 μm); (e) 10 wt% GNPs (magnification of 2000, scale bar of 10 μm); (f) 10 wt% GNPs (magnification of 5000, scale bar of 1 μm).

compared to that of pristine DGEBA. The electromagnetic shielding efficiency of the nanocomposite exhibited a maximum value of 3.87 dB at 10 wt% GNPs, which is 287% higher than that of pristine DGEBA. The fracture surfaces of the nanocomposites exhibited a rough morphology with numerous micro-cracks. In addition, the GNPs in the DGEBA matrix were stacked and formed a continuous conductive path at high GNP content.

ACKNOWLEDGEMENTS

This work was supported by the Technology Innovation Program (or Industrial Strategic Technology Development Program- Devel-

opment of technology on materials and components) (20010106, Adhesives with low water permeability and low outgassing) funded By the Ministry of Trade, Industry & Energy (MOTIE, Korea).

REFERENCES

1. M. Zhou, J. Wang, Y. Zhao, G. Wang, W. Gu and G. Ji, *Carbon*, **183**, 515 (2021).
2. D. D. L. Chung, *Mater. Chem. Phys.*, **255**, 123587 (2020).
3. W. Zhang, L. Wei, Z Ma, Q Fan and J Ma, *Carbon*, **177**, 412 (2021).
4. S. Sharma, B. P. Singh, S. S. Chauhan, J. Jyoti, A. K. Arya, S. R. Dhakate, V. Kumar and T. Yokozeki, *Compos. Part A-Appl. S.*, **104**, 129 (2018).
5. H. Lecocq, N. Garois, O. Lhost, P. F. Girard, P. Cassagnau and A. Serghei, *Compos. Part B-Eng.*, **189**, 107866 (2020).
6. D. Zhang, Y. Liao, S. Bandaru and X. Zhang, *J. Magn. Magn. Mater.*, **540**, 168434 (2021).
7. S. Liu, S. Qin, Y. Jiang, P. Song and H. Wang, *Compos. Part A-Appl. S.*, **145**, 106376 (2021).
8. J. Wang, R. Wu, J. Feng, J. Zhang, L. Hou and M. Zhang, *Mater. Charact.*, **157**, 109924 (2019).
9. X. Liu, H. Liu, H. Xu, W. Xie, M. Li, J. Liu, G. Liu, A. Weidenkaff and R. Riedel, *J. Colloid Interface Sci.*, **606**(2), 1543 (2021).
10. X. Jiang, C. Xu, T. Gao, Y. Bando, D. Golbeeerg, P. Dai, M. Hu, R. Ma, Z. Hu and X. B. Wang, *Compos. Commun.*, **25**, 100757 (2021).
11. M. Kasraie and P. P. S. S. Abadi, *Addit. Manuf.*, **46**, 102098 (2021).
12. A. P. Godoy, L. G. Amurim, A. Mendes, E. S. Gonçalves, A. Ferreira, C. S. Andrade, R. Kotsilkova, E. Ivanov, M. Lavorgna, L. A. M. Saito, H. Ribeiro and R. J. E. Andrade, *Prog. Org. Coat.*, **158**, 106341 (2021).
13. J. He, H. Zhang, Y. Chen, H. Zou and M. Liang, *React. Funct. Polym.*, **164**, 104918 (2021).
14. S. S. Yao, C. L. Ma, F. L. Jin and S. J. Park, *Korean J. Chem. Eng.*, **37**(11), 2075 (2020).
15. W. Li, J. Ma, S. Wu, J. Zhang and J. Cheng, *Polym. Test.*, **101**, 107275 (2021).
16. J. Chen, N. Chu, M. Zhao, F. L. Jin and S. J. Park, *J. Appl. Polym. Sci.*, **137**(48), 49592 (2020).
17. S. Liu, V. S. Chevali, Z. Xu, D. Hui and H. Wang, *Compos. Part B-Eng.*, **136**, 197 (2018).
18. Y. H. Bae, M. J. Yu, M. C. Vu, W. K. Choi and S. R. Kim, *Compos. Sci. Technol.*, **155**, 144 (2018).
19. L. Vovchenko, O. Lozitsky, L. Matzui, V. Oliynyk, V. Zagorodnii and M. Skoryk, *Mater. Chem. Phys.*, **240**, 122234 (2020).
20. J. Wang, C. Ma, G. Chen and P. Dai, *Compos. Struct.*, **234**, 111649 (2020).
21. N. Boumedienne and A. Maaroufi, *Physica B*, **578**, 411853 (2020).
22. Y. Li, J. Liu, S. Wang, L. Zhang and B. Shen, *Compos. Part B-Eng.*, **182**, 107615 (2020).
23. X. Xia, G. J. Weng, J. Xiao and W. Wen, *Mater. Today Commun.*, **22**, 100853 (2020).
24. X. Fan, Q. Gao, Y. Gao, G. Zhang, F. Huang, R. Xiao, W. Liu, F. Wang, J. Qin, E. Bilotti, H. Zhang, X. Shi and G. Zhang, *Compos. Sci. Technol.*, **215**, 109000 (2021).
25. A. Kumar, R. Anant, K. Kumar, S. S. Chauhan, S. Kumar and R. Kumar, *RSC Adv.*, **6**, 113405 (2016).
26. Q. Meng, H. Wu, Z. Zhao, S. Araby, S. Lu and J. Ma, *Compos. Part A-Appl. S.*, **92**, 42 (2017).
27. K. Wang, W. Wang, H. Wang, L. Liu, Z. Xu, H. Fu, L. Zhao, X. Zhang, L. Chen and Y. Zhao, *Compos. Part A-Appl. S.*, **110**, 246 (2018).
28. C. Arribas, M. G. Prolongo, M. Sáanchez-Cabezudo, R. Moriche and S. G. Prolongo, *Polym. Degrad. Stabil.*, **170**, 109003 (2019).
29. S. Han, Q. Meng, S. Araby, T. Liu and M. Demiral, *Compos. Part A-Appl. S.*, **120**, 116 (2019).
30. H. Liu, C. Liang, J. Chen, Y. Huang, F. Cheng, F. Wen, B. Xu and B. Wang, *Compos. Sci. Technol.*, **169**, 103 (2019).
31. Y. Huangfu, C. Liang, Y. Han, H. Qiu, P. Song, L. Wang, J. Kong and J. Gu, *Compos. Sci. Technol.*, **169**, 70 (2019).
32. Y. Chen, H. B. Zhang, M. Wang, X. Qian, A. Dasari and Z. Z. Yu, *Compos. Sci. Technol.*, **152**, 254 (2017).
33. M. A. Tarawneh, S. A. Saraireh, R. S. Chen, S. H. Ahmad, M. A. M. Al-Tarawni, L. J. Yu, B. O. Alsobhi and D. Hui, *Nanotechnol. Rev.*, **9**, 1550 (2020).
34. Q. Meng, V. Kenelak, A. Chand, H. Kang, S. Han and T. Liu, *J. Appl. Polym. Sci.*, **137**(34), 48991 (2020).
35. S. Wang, H. Xue, S. Guo, M. Cao, F. Cong, S. Araby and Q. Meng, *J. Appl. Polym. Sci.*, **138**(14), 50163 (2020).
36. Q. Meng, S. Araby, J. A. Oh, A. Chand, X. Zhang, V. Kenelak, J. Ma, T. Liu and J. Ma, *J. Appl. Polym. Sci.*, **138**(20), 50452 (2021).
37. H. Liu, C. Liang, J. Chen, Y. Huang, F. Cheng, F. Wen, B. Xu and B. Wang, *ACS Appl. Mater. Inter.*, **8**, 33230 (2016).
38. T. T. V. Tran, D. V. N. Vo, S. T. Nguyen and C. M. Vu, *Compos. Part A-Appl. S.*, **149**, 106485 (2021).
39. F. L. Jin, R. R. Hu and S. J. Park, *Korean J. Chem. Eng.*, **37**(5), 905 (2020).
40. J. Chen, R. R. Hu, F. L. Jin and S. J. Park, *J. Appl. Polym. Sci.*, **138**(16), 50250 (2021).
41. X. Yang, S. Fan, Y. Li, Y. Guo, Y. Li, K. Ruan, S. Zhang, J. Zhang, J. Kong and J. Gu, *Compos. Part A-Appl. S.*, **128**, 105670 (2020).
42. S. Chhetri, N. C. Adak, P. Samanta, N. C. Murmu, D. Hui, T. Kuila and J. H. Lee, *Compos. Part B-Eng.*, **143**, 105 (2018).
43. H. Wang, S. S. Yao, Z. Guan, F. L. Jin and S. J. Park, *Korean J. Chem. Eng.*, **38**(11), 2332 (2021).
44. F. L. Jin, C. L. Ma, B. T. Guo and S. J. Park, *Bull. Korean Chem. Soc.*, **40**(10), 991 (2019).
45. J. Peng, C. Huang, C. Cao, E. Saiz, Y. Du, S. Dou, A. P. Tomsia, H. D. Wagner, L. Jiang and Q. Cheng, *Matter*, **2**, 220 (2020).
46. K. Wang, W. Wang, H. Wang, L. Liu, Z. Xu, H. Fu, L. Zhao, X. Zhang, L. Chen and Y. Zhao, *Compos. Part A-Appl. S.*, **110**, 246 (2018).
47. R. Aradhana, S. Mohanty and S. K. Nayak, *Polymer*, **141**, 109 (2018).
48. H. Liu, C. Liang, J. Chen, Y. Huang, F. Cheng, F. Wen, B. Xu and B. Wang, *Compos. Sci. Technol.*, **169**, 103 (2019).
49. H. Duan, H. Zhu, J. Yang, J. Gao, Y. Yang, L. Xu, G. Zhao and Y. Liu, *Compos. Part A-Appl. S.*, **118**, 41 (2019).
50. S. Zhang, S. Yin, Q. Ran, Q. Fu and Y. Gu, *Polymer*, **162**, 20 (2019).
51. M. J. Kang, F. L. Jin and S. J. Park, *Macromol. Res.*, **26**(11), 1048 (2018).
52. A. Bisht, K. Dasgupta and D. Lahiri, *Polym. Test.*, **81**, 106274 (2020).
53. H. Zhang, G. Zhang, M. Tang, L. Zhou, J. Li, X. Fan, X. Shi and J. Qin, *Chem. Eng. J.*, **353**, 381 (2018).